

Received 10 February 2024, accepted 11 March 2024, date of publication 25 March 2024, date of current version 1 May 2024.

Digital Object Identifier 10.1109/ACCESS.2024.3381613

RESEARCH ARTICLE

Enhancing Fault Ride-Through Capacity of DFIG-Based WPs by Adaptive Backstepping Command Using Parametric Estimation in Non-Linear Forward Power Controller Design

AZEDDINE LOULIJAT¹, MOHAMED MAKHAD², ABDELILAH HILALI³, HAMID CHOJAA⁴,
MOUNCEF EL MARGHICHI⁵, MOHAMMED HATATAH⁶,
AND THAMER A. H. ALGHAMDI^{6,7}

¹Department of Electrical Engineering, Hassan 1st University, Settat 26000, Morocco

²Department of Electrical Engineering, Mohamed V University, Rabat 10120, Morocco

³Faculty of Sciences, Moulay Ismail University, Meknes 11201, Morocco

⁴Industrial Technologies and Services Laboratory, Higher School of Technology, Sidi Mohamed Ben Abdellah University, Fes 30000, Morocco

⁵Intelligent Systems Design Laboratory, Faculty of Sciences, Abdelmalek Essaadi University, Tetouan 39000, Morocco


⁶Electrical Engineering Department, Faculty of Engineering, Al-Baha University, Al-Baha 65779, Saudi Arabia

⁷Wolfson Centre for Magnetics, School of Engineering, Cardiff University, CF24 3AA Cardiff, U.K.

Corresponding authors: Azeddine Loulijat (rehalloulijat@gmail.com) and Thamer A. H. Alghamdi (Alghamdit1@cardiff.ac.uk)

ABSTRACT The principal issue associated with wind parks (WPs) based on doubly-fed induction generators (DFIGs) is their vulnerability to network faults. This paper presents a novel nonlinear forward power controller design with an adaptive backstepping command using parametric estimation (NFPC_ABC-PE) to enhance fault ride-through (FRT) capacities in WP utilizing DFIGs. The suggested NFPC_ABC-PE manipulates both rotor and network-side power converters (i.e., RSPCs and NSPCs). Specifically, RSPCs are manipulated to maintain the targeted voltage at dc-bus terminals, while NSPCs are manipulated to supply the reactive energy (power) necessary if the network is disturbed. As a result, the NFPC_ABC-PE proposed precisely supplies reactive energy to ensure the smooth execution of FRT ability. The method developed comprehends the dynamics of RSPC, NSPC-side filters, and dc-bus terminal voltage in the form of electrical active and reactive output power. The parameters of the RSPC and NSPC-side filters, including those associated with the dc-bus capacitor, are regarded as entirely unknown. To estimate and regulate these parameters, adaptation algorithms are utilized. The NFPC_ABC-PE employs parameter adaptation algorithms and switching control inputs designed to safeguard the overall stability of WP. The stability analysis of the DFIG-based WPs with the proposed NFPC_ABC-PE involves applying stability in the sense of the Lyapunov function (LF). To validate its efficacy, simulations are carried out on a single 10 MW power generation unit. The results of the simulation highlight a clear enhancement in the stability and FRT capability of WP, contrasting with the nonlinear forward power controller employing the sliding mode command (NFPC-SMC).

INDEX TERMS WPs, DFIG, network code, FRT, parametric estimation, NFPC_ABC, LF, NFPC-SMC.

The associate editor coordinating the review of this manuscript and approving it for publication was Tariq Masood .

I. INTRODUCTION

The technical advantages offered by doubly-fed induction generators (DFIG)-based wind parks (WPs) make them the

preferred choice [1]. These WPs are characterized by their capability to operate efficiently at diverse wind speeds and their capacity for reactive power to maintain voltage stability. In adherence to the network code, the WPs are obligated to connect to the network in instances of defaults or voltage drops caused by external perturbations. In such situations, WPs need additional reactive power support to maintain the tension stability of the entire system. Failure to manage these events effectively can lead to blackouts [2]. Additionally, in order to protect against overvoltage, it is crucial to ensure that the dc-bus voltage is maintained via the capacitor. The capacity of WPs to link with the main network amid fault conditions is referred to as fault ride-through (FRT) capacity [3]. In WPs based on DFIG, the network-side power converter (NSPC) furnishes reactive power supplies, while both the NSPC and rotor-side power converter (RSPC) are utilized to uphold the required dc-bus tension through maintaining an adequate power equalization between the two converters. Hence, it is crucial to formulate regulators for the converters (specifically, the NSPC and RSPC) to guarantee the stability, i.e., FRT function, of WPs employing DFIGs.

Improving the FRT capacities of DFIG-based WPs can be accomplished through three main approaches: employing protective measures (such as a crowbar) or devices for injecting reactive energy (such as static synchronous compensators), and adjusting the switching command signals for the two converters [4]. The crowbar device, described in [5], safeguards the RSPC during faults but causes DFIGs to function as squirrel cage induction generators (SCIGs), absorbing reactive energy and degrading network voltage. The integration of a crowbar with a series R-L setup, demonstrated in [6] and [7], aims to improve conventional crowbar performance by turning the DFIG-based wind turbine into a hybrid system combining features of both a DFIG and a SCIG. While it enhances performance, it falls short of delivering the required reactive energy supplies to guarantee FRT operation as stipulated by the network code. In [8], [9], and [10], the DC-link chopper device is utilized to address overvoltage concerns in the dc-bus, providing protection to the rotor in a manner similar to the crowbar. Combining DC-link choppers with series dynamic braking resistors [11], [12], superconducting magnets [13], and superconducting fault current limiters [14], [15] are employed to enhance the FRT functions of DFIG-based WPs. The utilization of the DC-link chopper, in conjunction with related devices, enables DFIG-based WPs to retain consistent characteristics, ensuring that DFIGs do not manifest the traits of SCIGs. Nevertheless, an excess current persists at the rotor, flowing along the diode, and the time required to attain the steady state after the fault is longer than with the crowbar [16].

The widespread use of Flexible Alternating Current Transmission System (FACTS) equipment in DFIG-based WPs aims to enhance FRT capabilities by supplying reactive energy externally. Series compensators, such as dynamic voltage restorers [17], [18], [19], are commonly utilized to

improve FRT capacities in WPs. However, the introduction of subsynchronous oscillations by these compensators emphasizes the need for additional precautions to mitigate such oscillations [20]. To maintain voltage stability in DFIG-based wind power systems, various shunt FACTS devices, including static synchronous compensators and static var compensators, are employed [21], [22], [23]. Nonetheless, integrating these FACTS devices adds complexity to the network and incurs additional costs. Adjusting the internal commands of RSPCs and NSPCs within these WPs can be a viable alternative to ensure FRT functionality, thereby eliminating the need for extra devices.

In [24], [25], and [26], vector command schemes employing proportional-integral and proportional-derivative regulators are implemented to improve the FRT capacity of DFIG-based WPs. Nevertheless, achieving optimal stability necessitates the precise tuning of gain parameters for these schemes, a task rendered challenging by the swift fluctuations in wind speed. The hysteresis command, as outlined in [27], is capable of generating optimal switching signal input for both RSPCs and NSPCs. Nevertheless, the primary issue associated with the hysteresis command lies in its variable switching frequency, which adds complexity to the filter design procedure. The enhancement of FRT performance in wind generation systems based on DFIG is achieved through the application of a control scheme based on a linear quadratic regulator, as outlined in [28]. Nevertheless, the effectiveness of this controller type is constrained to a limited set of operating points due to its reliance on linearized models of DFIGs during the design process.

Using nonlinear models, commands designed for DFIG-based wind turbines play a crucial role in ensuring FRT operation across a wide operating band. The paper [29], introduces a nonlinear backstepping command scheme aimed at improving the low-voltage ride-through (LVRT) ability of wind turbines based on DFIG in the presence of network faults. However, the backstepping algorithm outlined in [29] lacks robustness when confronted with outside perturbations and parametric uncertainties. Command nonlinear by sliding mode (SMC) are detailed in [30] for the same purposes. Nevertheless, chattering arises in the SMC due to the presence of non-modelled dynamics in DFIG-based WPs. However, these types of controllers employ currents as output values to monitor both active and reactive output power indirectly, with the goal of enhancing FRT capacity, despite the feasibility of achieving this more directly through direct power control.

The paper [31] introduces a nonlinear SMC for controlling active and reactive power in DFIG-based WPs. However, it still requires current measurement to execute power commands. And, in [32] utilizes a direct power control scheme via nonlinear backstepping without needing current measurements, focusing solely on active and reactive power dynamics. In contrast, the method described in [31] is sensitive to alterations in system components.

This research paper introduces a nonlinear forward power controller designed for RSPC and NSPC-side filters in DFIG-based wind power systems. It leverages an adaptive backstepping command, particularly useful for parameter estimation in cases where the parameters are entirely unknown. The developed scheme proficiently controls and regulates active and reactive power at RSPCs and NSPCs, alongside overseeing the DC-bus voltage. Ensures that WP's connection to the main network is maintained during a symmetrical three-phase short-circuit in the electrical network, by supplying the reactive power needed to restore voltage at the NIP. Simultaneously, adaptation algorithms are designed to deduce system parameters, assuming that these parameters are regarded as fully unidentified. The command and parameter adaptation algorithms are formulated to achieve the comprehensive stability of wind power systems incorporating DFIGs. Command in the sense of the Lyapunov function (LF), defining the system's energy, is utilized for the stability analysis. The effectiveness of the proposed NFPC_ABC-PE is evaluated within a network integrated with a wind energy system utilizing DFIGs. This evaluation highlights its superior performance across various metrics including injected reactive power, voltage restoration at the NIP, limitation of stator and rotor currents, and maintenance of the DC-bus voltage. The NFPC_ABC-PE approach is subjected to comprehensive assessment through simulation, contrasting its results with those obtained in the literature using an established control method, specifically the Nonlinear Forward Power Controller with Sliding Mode Control (NFPC_SMC). Through this evaluation, the NFPC_ABC-PE demonstrates its capability to effectively manage and optimize the operation of the wind energy system. Its superiority over the NFPC_SMC is evident in terms of its ability to enhance reactive power injection, facilitate voltage stabilization, minimize current fluctuations, and ensure stable dc-bus voltage levels. This comparison underscores the potential of the NFPC_ABC-PE as a promising control strategy for enhancing FRT Capacity of DFIG-based WPs.

The document follows the following organization. Section II provides an informative overview of the network code used. Section III is dedicated to modeling the RSPC and NSPC-side filters in terms of power with parameters completely unknown, and section IV also covers the synthesis of command laws by NFPC_ABC-PE. The results of the MATLAB/SIMULINK simulation evaluation and subsequent performance comparison are documented in Section V. The document is ultimately concluded in Section VI.

II. PROPRIETARY NETWORK CODE

WPs are now obligated by recent network codes to stay linked and assist the network both during and after a default. They need to endure voltage drops at a designated percentage of the typical voltage for specified durations, as indicated in the voltage-time transition profiles for LVRT as seen in Figure 1. It is prohibited to disconnect beyond the defined limit, and the WPs remain to be linked even if the voltage at the network

interconnection point (NIP) decreases to zero. WPs are not obligated to support the network below the defined limit, and protection switches can be activated after a 200 ms time delay to cut them off.

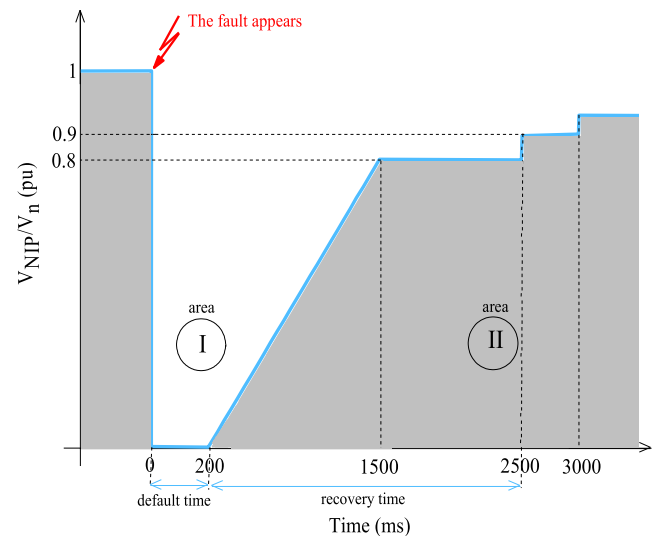


FIGURE 1. Network code specifications at NIP [33].

In Figure 1, Area I (white area) denotes absolutely no tripping, allowing the WPs to remain connected to the network, even in cases where the voltage at the NIP is zero. Area II (grey area) corresponds to the activation of the WPs' protection switches (disconnect).

III. DYNAMIC MODELING OF RSPC AND NSPC-SIDE FILTERS IN TERMS OF POWER WITH ENTIRELY UNKNOWN PARAMETERS

In this document, the suggested NFPC_ABC-PE is designed to directly monitor both active and reactive power through the precise command of the switching operations of the RSPC and NSPC. Hence, it is essential to formulate dynamic behavior models for the RSPC and NSPC-side filters that explicitly describe their behavior in terms of both active and reactive power. In Figure 2, a WP with a DFIG-based configuration is depicted, where a DFIG is connected to a WT via a multiplier (gearbox). The stator of the DFIG is then linked to the network through a power transformer and transport cable. The network electrical connection for the rotor output is established through a back-to-back power converter with two filters (r_{rf} , l_{rf} , r_{nf} and l_{nf}), incorporating a RSPC and NSPC cross-coupled by a dc-bus condenser (c_{dc}). This section focuses on formulating the dynamic models of the RSPC and NSPC-side filters, taken from the direct and quadrature components (d - and q -components) of current dynamics assigned with these converters. Additionally, the design process of the controller considers the dynamics of the dc-bus condenser, recognizing its crucial role in achieving the prescribed control goals.

After implementing the law of mailles on the circuit shown in Figure 3, we proceed to utilize the Park

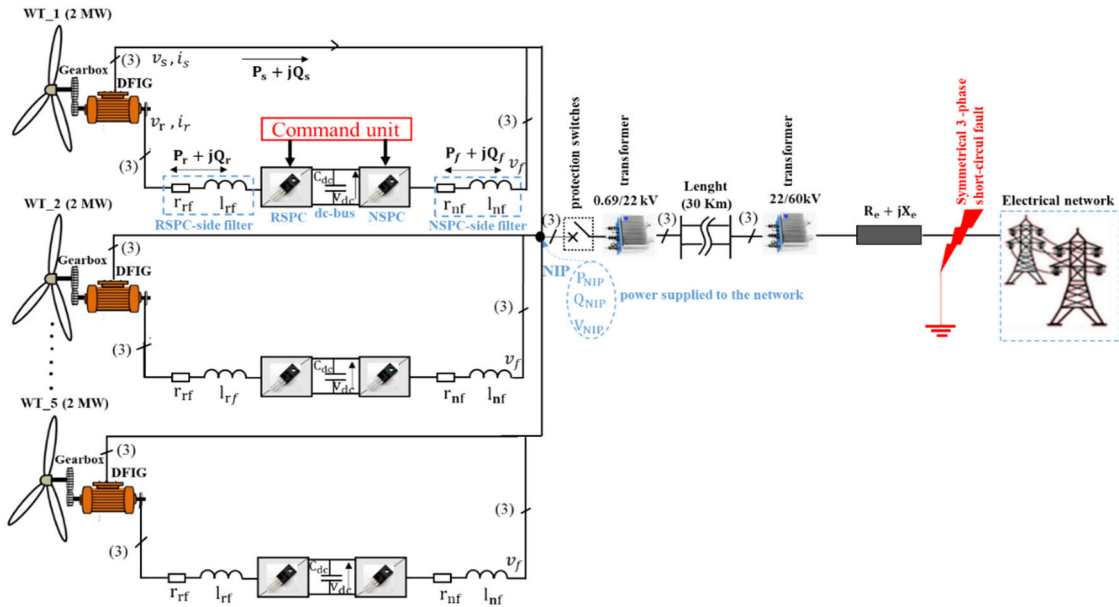


FIGURE 2. A wind energy system connected to the electrical network equipped with a DFIG.

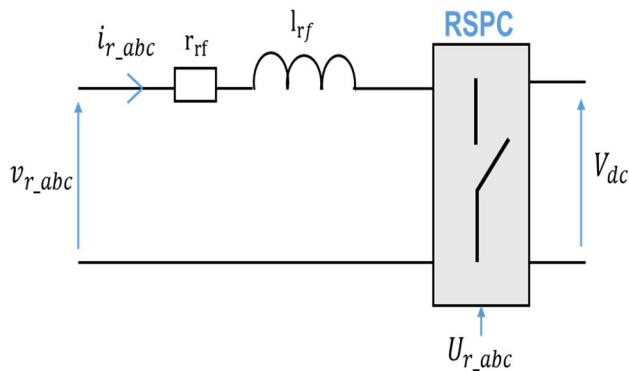


FIGURE 3. RSPC-side filter electrical circuit.

transform on the equations within the original reference frame (abc). The equations describing the dynamics of the d - and q -components currents related to the RSPC-side filter are written in (1) [34]:

$$\begin{cases} \frac{di_{rd}}{dt} = -\frac{r_{rf}}{l_{rf}}i_{rd} - \omega_s i_{rq} - \frac{V_{dc}}{l_{rf}}U_{rd} + \frac{v_{rd}}{l_{rf}} \\ \frac{di_{rq}}{dt} = -\frac{r_{rf}}{l_{rf}}i_{rq} + \omega_s i_{rd} - \frac{V_{dc}}{l_{rf}}U_{rq} + \frac{v_{rq}}{l_{rf}} \end{cases} \quad (1)$$

where i_{rd} denotes the d -component of rotor current in the Park reference frame, r_{rf} and l_{rf} write the resistance and inductance of the RSPC-side filter, ω_s is the rotational speed of the rotating reference, i_{rq} denotes the q -component of rotor current in the Park reference frame, V_{dc} is the voltage between the dc-bus, U_{rd} is the commutation signal for the d -component of the RSPC, v_{rd} represent the d -component in the Park reference frame of the rotor voltage, U_{rq} is the commutation signal for the q -component of the RSPC, and

v_{rq} represent the q -component in the Park reference frame of the rotor voltage.

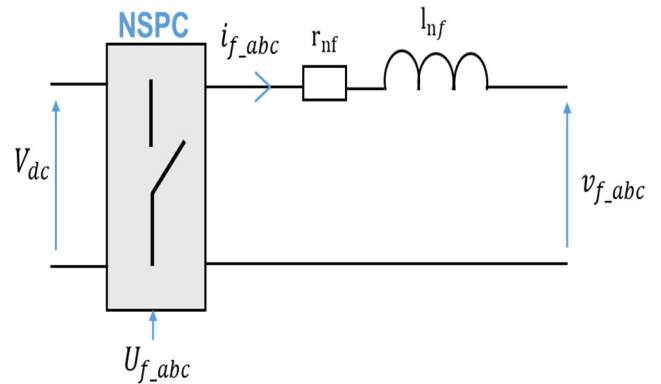


FIGURE 4. NSPC-side filter electrical circuit.

A similar process is used for the circuit shown in Figure 4, the behavior of d - and q -components currents across the NSPC-side filter can be expressed in (2) [34]:

$$\begin{cases} \frac{di_{fd}}{dt} = -\frac{r_{nf}}{l_{nf}}i_{fd} - \omega_s i_{fq} - \frac{V_{dc}}{l_{nf}}U_{fd} + \frac{v_{fd}}{l_{nf}} \\ \frac{di_{fq}}{dt} = -\frac{r_{nf}}{l_{nf}}i_{fq} + \omega_s i_{fd} - \frac{V_{dc}}{l_{nf}}U_{fq} + \frac{v_{fq}}{l_{nf}} \end{cases} \quad (2)$$

where i_{fd} and i_{fq} refers the d - and q -components of current in the Park reference frame passing through the NSPC-side filter, r_{nf} and l_{nf} write the resistance and inductance of the NSPC-side filter, U_{fd} and U_{fq} is the commutation signals for the d - and q -components of the NSPC. Finally, v_{fd} and v_{fq} represent the d - and q -components in the Park reference frame of the NSPC-side filter voltage.

The RSPC's active (P_r) and reactive (Q_r) power output can be articulated in terms of the d - and q -components of currents and voltages, expressed as follows [35]:

$$\begin{cases} P_r = 1.5(v_{rd}i_{rd} + v_{rq}i_{rq}) \\ Q_r = 1.5(v_{rd}i_{rq} - v_{rq}i_{rd}) \end{cases} \quad (3)$$

In the same way, the active (P_f) and reactive (Q_f) power delivered from the NSPC to the network can be expressed in terms of the corresponding d - and q -components of currents and voltages, expressed as follows [35]:

$$\begin{cases} P_f = 1.5(v_{fd}i_{fd} + v_{fq}i_{fq}) \\ Q_f = 1.5(v_{fd}i_{fq} - v_{fq}i_{fd}) \end{cases} \quad (4)$$

Equations (1)-(4) can be employed to address the interactions of the RSPC and NSPC in relation to pertinent active and reactive power. Deriving (3) and (4) and incorporating (1) and (2) allows for the formulation of simplified expressions describing the dynamics of the RSPC and NSPC in relation to appropriate active and reactive power. These simplified equations can be written as follows:

$$\begin{cases} \dot{P}_r = -\frac{r_{rf}}{l_{rf}}P_r - \omega_s Q_r - \frac{1.5}{l_{rf}}(v_{rd}V_{dc}U_{rd} + v_{rq}V_{dc}U_{rq} - v_{rd}^2 - v_{rq}^2) \\ \dot{Q}_r = -\frac{r_{rf}}{l_{rf}}Q_r + \omega_s P_r - \frac{1.5}{l_{rf}}(v_{rd}V_{dc}U_{rq} + v_{rq}V_{dc}U_{rd}) \\ \dot{P}_f = -\frac{r_{nf}}{l_{nf}}P_f - \omega_s Q_f - \frac{1.5}{l_{nf}}(v_{fd}V_{dc}U_{fd} + v_{fq}V_{dc}U_{fq} - v_{fd}^2 - v_{fq}^2) \\ \dot{Q}_f = -\frac{r_{nf}}{l_{nf}}Q_f + \omega_s P_f - \frac{1.5}{l_{nf}}(v_{fd}V_{dc}U_{fq} + v_{fq}V_{dc}U_{fd}) \end{cases} \quad (5)$$

In this research, the focus is on monitoring the dc-bus voltage to ensure its desired level is upheld consistently, even in the presence of faults or other types of operating conditions. The formulation of the dc-bus voltage evolution, as expressed in (6), is extracted from Figure 5, depicting a power circuit integrated with the dc-bus, by applying the law of nodes in the power sense with all losses due to Joule effect neglected [6]:

$$\begin{cases} P_{dc} = P_r - P_f = \frac{d}{dt} \left(\underbrace{\frac{1}{2}c_{dc}V_{dc}^2}_{\text{Energy stored in dc-bus condenser}} \right) \\ = c_{dc}V_{dc}\dot{V}_{dc} \\ \dot{V}_{dc} = \frac{1}{c_{dc}V_{dc}}(P_r - P_f) \end{cases} \quad (6)$$

Based on (5) and (6), in terms of active and reactive power, the complete state system of DFIG-based WPs can be

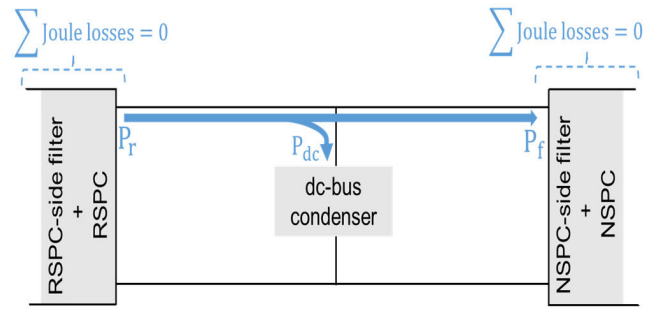


FIGURE 5. Dc-bus model in direction of power transfer.

expressed as follows:

$$\begin{cases} \dot{V}_{dc} = \frac{1}{c_{dc}V_{dc}}(P_r - P_f) \\ \dot{P}_r = -\frac{r_{rf}}{l_{rf}}P_r - \omega_s Q_r - \frac{1.5}{l_{rf}}(v_{rd}V_{dc}U_{rd} + v_{rq}V_{dc}U_{rq} - v_{rd}^2 - v_{rq}^2) \\ \dot{Q}_r = -\frac{r_{rf}}{l_{rf}}Q_r + \omega_s P_r - \frac{1.5}{l_{rf}}(v_{rd}V_{dc}U_{rq} + v_{rq}V_{dc}U_{rd}) \\ \dot{P}_f = -\frac{r_{nf}}{l_{nf}}P_f - \omega_s Q_f - \frac{1.5}{l_{nf}}(v_{fd}V_{dc}U_{fd} + v_{fq}V_{dc}U_{fq} - v_{fd}^2 - v_{fq}^2) \\ \dot{Q}_f = -\frac{r_{nf}}{l_{nf}}Q_f + \omega_s P_f - \frac{1.5}{l_{nf}}(v_{fd}V_{dc}U_{fq} + v_{fq}V_{dc}U_{fd}) \end{cases} \quad (7)$$

If the d -component of the synchronously rotating direct-quadrature frame is taken as the baseline frame, coincident with both the network and rotor voltage vectors, the q -components of the filter and rotor voltages will be removed, i.e. $v_{rq} = 0$ and $v_{fq} = 0$. Therefore, equation (7) becomes simplified as follows:

$$\begin{cases} \dot{V}_{dc} = \frac{1}{c_{dc}V_{dc}}(P_r - P_f) \\ \dot{P}_r = -\frac{r_{rf}}{l_{rf}}P_r - \omega_s Q_r - \frac{1.5}{l_{rf}}(v_{rd}V_{dc}U_{rd} - v_{rd}^2) \\ \dot{Q}_r = -\frac{r_{rf}}{l_{rf}}Q_r + \omega_s P_r - \frac{1.5}{l_{rf}}v_{rd}V_{dc}U_{rq} \\ \dot{P}_f = -\frac{r_{nf}}{l_{nf}}P_f - \omega_s Q_f - \frac{1.5}{l_{nf}}(v_{fd}V_{dc}U_{fd} - v_{fd}^2) \\ \dot{Q}_f = -\frac{r_{nf}}{l_{nf}}Q_f + \omega_s P_f - \frac{1.5}{l_{nf}}v_{fd}V_{dc}U_{fq} \end{cases} \quad (8)$$

The design of the proposed NFPC_ABC-PE for both RSPC and NSPC-side filters is based on the state model described by the equation system in (8). The dynamics of the active and reactive power in both RSPC and NSPC-side filters are influenced by the filter parameters (r_{rf} , l_{rf} , r_{nf} , and l_{nf}), as indicated in equation system in (8). Additionally, the dynamics of the dc-bus voltage are impacted by the presence of the dc-bus condenser (c_{dc}). For the model-based controllers to be effectively implemented, it is necessary to have precise knowledge of the parameters within the model, as the performance is

directly influenced by the sensitivity of these parameters. But, acquiring precise parametric information for DFIG-WPs proves to be a challenging task. The proposed non-linear forward controller design of power scheme enables the treatment of all parameters in (8) as complete unknowns, and they can be expressed as follows:

$$d_0 = \frac{1}{c_{dc}}, \quad d_1 = \frac{r_{rf}}{l_{rf}}, \quad d_2 = \frac{1.5}{l_{rf}}, \quad d_3 = \frac{r_{nf}}{l_{nf}} \quad \& \quad d_4 = \frac{1.5}{l_{nf}}$$

The unknown parameters, denoted as $d_0, d_1, d_2, d_3,$ and $d_4,$ are employed in rewriting (8) as follows:

$$\begin{cases} \dot{V}_{dc} = \frac{d_0}{V_{dc}}(P_r - P_f) \\ \dot{P}_r = -d_1 P_r - \omega_s Q_r - d_2(v_{rd} V_{dc} U_{rd} - v_{rd}^2) \\ \dot{Q}_r = -d_1 Q_r + \omega_s P_r - d_2 v_{rd} V_{dc} U_{rq} \\ \dot{P}_f = -d_3 P_f - \omega_s Q_f - d_4(v_{fd} V_{dc} U_{fd} - v_{fd}^2) \\ \dot{Q}_f = -d_3 Q_f + \omega_s P_f - d_4 v_{fd} V_{dc} U_{fq} \end{cases} \quad (9)$$

The proposed NFPC_ABC-PE are formulated based on the models defined in equation specification (9), where adaptation algorithms are employed to estimate all unknown parameters. The commutation command signals are then utilized to improve the FRT capacity of DFIG used in WPs.

IV. SYNTHESIS OF COMMAND LAWS

The developed NFPC_ABC-PE is configured to ensure the global stability of the wind energy production system with DFIGs through the integration of commutation command signals and parameter adaptation algorithms. The NFPC_ABC-PE proposed guarantees precise tracking of all variable states, including $V_{dc}, P_r, Q_r, P_f,$ and $Q_f.$ The subsequent discussion outlines the steps pertaining to the proposed NFPC_ABC-PE concept.

Step 1: The intended dc-bus voltage (V_{dc}) is identified as V_{dc}^* , and the associated pursuit tracking (ε_0) for the dc-bus voltage can be expressed as follows:

$$\varepsilon_0 = V_{dc} - V_{dc}^* \quad (10)$$

And the evolution of this error can be presented as its derivative as shown below:

$$\dot{\varepsilon}_0 = \frac{d_0}{V_{dc}}(P_r - P_f) \quad (11)$$

Given the presence of the unknown parameter (d_0) in (11), it can be substituted with the estimation error (\tilde{d}_0) and its estimated state value (\hat{d}_0), as demonstrated in the next equation:

$$\dot{\varepsilon}_0 = \frac{(\tilde{d}_0 + \hat{d}_0)}{V_{dc}}(P_r - P_f) \quad (12)$$

where $\tilde{d}_0 = d_0 - \hat{d}_0.$ Zero pursuit tracking error is attainable when V_{dc} approaches V_{dc}^* (denoted as $V_{dc} \rightarrow V_{dc}^*$). This can be examined by formulating a LF, as presented in the subsequent equation:

$$V_0(\varepsilon_0, \tilde{d}_0) = \frac{1}{2}\varepsilon_0^2 + \frac{1}{2\beta_0}\tilde{d}_0^2 \quad (13)$$

β_0 is a fixed positive constant, also called the gain of adaptation. This is commonly utilized to accelerate the error's convergence towards its target value. So, if we differentiate V_0 and substitute the derivative value of ε_0 from (11), the expression becomes as follows:

$$\begin{aligned} \dot{V}_0(\varepsilon_0, \tilde{d}_0) &= \varepsilon_0 \left(\frac{d_0}{V_{dc}}(P_r - P_f) \right) - \frac{\tilde{d}_0}{\beta_0} \left(\dot{\tilde{d}}_0 - \varepsilon_0 \frac{\beta_0}{V_{dc}}(P_r - P_f) \right) \end{aligned} \quad (14)$$

The system will secure the targeted tracking of ε_1 and maintain stability once $\dot{V}_0 < 0$ or $\dot{V}_0 \leq 0.$ Given that (14) does not incorporate the actual commutation command signals, it is imperative to opt for virtual command inputs, represented as δ_0 for P_r and δ_1 for $P_f,$ respectively. The selection of these stabilizing functions can be done in the following manner:

$$\begin{cases} \delta_0 = \frac{V_{dc}}{\hat{d}_0} \\ \delta_1 = \frac{V_{dc}}{\hat{d}_0}(1 + c_0\varepsilon_0) \end{cases} \quad (15)$$

Here, a positive design parameter, denoted as $c_0 > 0,$ is chosen to guarantee the targeted speed of convergence of $\varepsilon_0.$ As (14) lacks commutation command signals, there is no development of a parameter estimator to estimate d at this time. However, to remedy the poor signal, a tuning setting (μ) is added in the following form:

$$\mu = \frac{\varepsilon_0\beta_0}{V_{dc}}(P_r - P_f) \quad (16)$$

With the application of this setting parameter, (14) can be expressed more simply as:

$$\dot{V}_0(\varepsilon_0, \tilde{d}_0) = -c_0\varepsilon_0^2 - \frac{\tilde{d}_0}{\beta_0}(\dot{\tilde{d}}_0 - \mu) \quad (17)$$

The presence of the first term in (17) specifies a negative definite or pseudo-definite nature, whereas the adjustment function changes the second term. In the next step, through the appropriateness use of the associated adaptation algorithm, this second term will be nullified.

At this time, it is important to determine δ_0 and $\delta_1,$ as they will play a key role in analyzing dynamics of the error assigned to P_r and P_f in the subsequent step. In the simplified format below, the quantities of δ_0 and δ_1 can be expressed as a simple formula:

$$\begin{cases} \dot{\delta}_0 = M_0 d_0 - N_0 \\ \dot{\delta}_1 = M_1 d_0 - N_1 \end{cases} \quad (18)$$

With:

$$\begin{cases} M_0 = \frac{1}{\hat{d}_0 V_{dc}} (P_r - P_f) \\ N_0 = \frac{\hat{d}_0}{\hat{d}_0^2} V_{dc} \\ M_1 = M_0 + \frac{c_0}{\hat{d}_0} (P_r - P_f)(\varepsilon_0 + V_{dc}) \\ N_1 = N_0 + \frac{c_0 \varepsilon_0}{\hat{d}_0^2} V_{dc} \end{cases}$$

Additional error dynamics are scrutinized for convergence, along with the configuration of NFPC_ABC-PE and the establishment of adaptation algorithms.

Step 2: The errors (ε) associated with the other four participating variables (P_r , Q_r , P_f , and Q_f) in (9) can be formulated as follows:

$$\begin{cases} \varepsilon_1 = P_r - \delta_0 \\ \varepsilon_2 = Q_r - Q_r^* \\ \varepsilon_3 = P_f - \delta_1 \\ \varepsilon_4 = Q_f - Q_f^* \end{cases} \quad (19)$$

In this context, Q_r^* indicates the preferred reactive power at the RSPC-side filter, while Q_f^* indicates the preferred reactive power at the NSPC-side filter. Utilizing (9) together with (18), the dynamics of the errors in (19) can be formulated as follows:

$$\begin{cases} \dot{\varepsilon}_1 = -d_1 P_r - \omega_s Q_r - d_2 (v_{rd} V_{dc} U_{rd} - v_{rd}^2) - M_0 \dot{d}_0 + N_0 \\ \dot{\varepsilon}_2 = -d_1 Q_r + \omega_s P_r - d_2 v_{rd} V_{dc} U_{rq} - \dot{Q}_r^* \\ \dot{\varepsilon}_3 = -d_3 P_f - \omega_s Q_f - d_4 (v_{fd} V_{dc} U_{fd} - v_{fd}^2) - M_1 \dot{d}_0 + N_1 \\ \dot{\varepsilon}_4 = -d_3 Q_f + \omega_s P_f - d_4 v_{fd} V_{dc} U_{fq} - \dot{Q}_f^* \end{cases} \quad (20)$$

Equation (20) allows for the representation of the unidentified parameters (d_0 , d_1 , d_2 , d_3 , and d_4) in relation to their associated errors of estimation (\tilde{d}_0 , \tilde{d}_1 , \tilde{d}_2 , \tilde{d}_3 and \tilde{d}_4) and values from estimates (\hat{d}_0 , \hat{d}_1 , \hat{d}_2 , \hat{d}_3 and \hat{d}_4). The relationship is expressed by the formula: $\tilde{d}_i = d_i - \hat{d}_i$, where i ranges from 0 to 4.

$$\begin{cases} \dot{\varepsilon}_1 = -(\tilde{d}_1 + \hat{d}_1) P_r - \omega_s Q_r - (\tilde{d}_2 + \hat{d}_2) (v_{rd} V_{dc} U_{rd} - v_{rd}^2) - M_0 (\tilde{d}_0 + \hat{d}_0) + N_0 \\ \dot{\varepsilon}_2 = -(\tilde{d}_1 + \hat{d}_1) Q_r + \omega_s P_r - (\tilde{d}_2 + \hat{d}_2) v_{rd} V_{dc} U_{rq} - \dot{Q}_r^* \\ \dot{\varepsilon}_3 = -(\tilde{d}_3 + \hat{d}_3) P_f - \omega_s Q_f - (\tilde{d}_4 + \hat{d}_4) (v_{fd} V_{dc} U_{fd} - v_{fd}^2) - M_1 (\tilde{d}_0 + \hat{d}_0) + N_1 \\ \dot{\varepsilon}_4 = -(\tilde{d}_3 + \hat{d}_3) Q_f + \omega_s P_f - (\tilde{d}_4 + \hat{d}_4) v_{fd} V_{dc} U_{fq} - \dot{Q}_f^* \end{cases} \quad (21)$$

We can see in (21) the presence of the initial control outputs (U_{rd} , U_{rq} , U_{fd} and U_{fq}), which suggests that they are likely to cause all the errors in reaching convergence. Furthermore, the adaptation algorithms are required to ensure the target estimation of the values of the not known parameters. For both, the overall stability of the entire system needs to be preserved. On the basis of these situations, the

stability of WPs based on the DFIG can be verified using the following LF:

$$V_1(\varepsilon_i, \tilde{d}_i) = V_0(\varepsilon_0, \tilde{d}_0) + \frac{1}{2} \sum_{i=1}^{i=4} \varepsilon_i^2 + \frac{1}{2} \sum_{i=1}^{i=4} \frac{\tilde{d}_i^2}{\beta_i} \quad (22)$$

The settings adaptation gains are denoted by β_i , where i takes values from 1 to 4. Upon replacing the values of $\dot{V}_0(\varepsilon_0, \tilde{d}_0)$ from (17) and $\dot{\varepsilon}_1, \dot{\varepsilon}_2, \dot{\varepsilon}_3$, and $\dot{\varepsilon}_4$ from (21), the derivative of $V_1(\varepsilon_i, \tilde{d}_i)$ in (22) can be expressed as follows (23), shown at the bottom of the next page.

The impacts of \tilde{d}_0 , \tilde{d}_1 , \tilde{d}_2 , \tilde{d}_3 and \tilde{d}_4 in (23) can be removed by opting for the choice of the following setting estimators or adaptation algorithms:

$$\begin{cases} \dot{\tilde{d}}_0 = \mu - \beta_0 (M_0 \varepsilon_1 + M_1 \varepsilon_3) \\ \dot{\tilde{d}}_1 = -\beta_1 (\varepsilon_1 P_r + \varepsilon_2 Q_r) \\ \dot{\tilde{d}}_2 = -\beta_2 (\varepsilon_1 (v_{rd} V_{dc} U_{rd} - v_{rd}^2) + \varepsilon_2 v_{rd} V_{dc} U_{rq}) \\ \dot{\tilde{d}}_3 = -\beta_3 (\varepsilon_3 P_f + \varepsilon_4 Q_f) \\ \dot{\tilde{d}}_4 = -\beta_4 (\varepsilon_3 (v_{fd} V_{dc} U_{fd} - v_{fd}^2) + \varepsilon_4 v_{fd} V_{dc} U_{fq}) \end{cases} \quad (24)$$

These adaptation algorithms simplify (23), as it appears at the end of the page, into (25), shown at the bottom of the next page.

At this time, the command signals for the RSPC and NSPC must be configured in a manner that ensures $\dot{V}_1(\varepsilon_i, \tilde{d}_i) < 0$ or $\dot{V}_1(\varepsilon_i, \tilde{d}_i) \leq 0$, a condition met only when opting for the following values for U_{rd} , U_{rq} , U_{fd} , and U_{fq} :

$$\begin{cases} U_{rd} = \frac{\hat{d}_2 v_{rd}^2 - \hat{d}_1 P_r - \omega_s Q_r - M_0 \hat{d}_0 + N_0 + c_1 \varepsilon_1}{\hat{d}_2 v_{rd} V_{dc}} \\ U_{rq} = \frac{P_r \omega_s - \hat{d}_1 Q_r - Q_r^* + c_2 \varepsilon_2}{\hat{d}_2 v_{rd} V_{dc}} \\ U_{fd} = \frac{\hat{d}_4 v_{fd}^2 - \hat{d}_3 P_f - \omega_s Q_f - M_1 \hat{d}_0 + N_1 + c_3 \varepsilon_3}{\hat{d}_4 v_{fd} V_{dc}} \\ U_{fq} = \frac{P_f \omega_s - \hat{d}_3 Q_f - Q_f^* + c_4 \varepsilon_4}{\hat{d}_4 v_{fd} V_{dc}} \end{cases} \quad (26)$$

In the equation, c_1 , c_2 , c_3 , and c_4 are positive conception factors. With the application of the command signals for the RSPC and NSPC as outlined in (26), equation (25) can be expressed in a simplified form:

$$\dot{V}_1(\varepsilon_i, \tilde{d}_i) = -c_0 \varepsilon_0^2 - c_1 \varepsilon_1^2 - c_2 \varepsilon_2^2 - c_3 \varepsilon_3^2 - c_4 \varepsilon_4^2 \leq 0 \quad (27)$$

As indicated by (27), it is evident that $\dot{V}_1(\varepsilon_i, \tilde{d}_i)$ attains negative semi-definiteness when all errors tend to zero. This confirms that the stability of the overall system is guaranteed by the adaptation and commutation command inputs conceived. The synoptic scheme of the command strategy of the RSPC and NSPC-side filters is shown in Figure 6.

V. RESEARCH RESULTS AND DISCUSSIONS

The NFPC_ABC-PE conceived for the RSPC and NSPC-side filters are evaluated in terms of performance on a WP resembling the one depicted in Figure 2. The WP illustrated in Figure 2, based on DFIG technology, depicts a collective configuration comprising five units, each with a rated output of 2 MW, interconnected to the network. A list of DFIG settings values is available in Table 1 [6]. In the DFIG-based dynamic model of the wind energy production unit, various parameters are present, encompassing the dc-bus condenser, resistances, and inductances for both the RSPC and NSPC-side filters.

These parameters are treated as not known and are automatically estimated through the use of adaptation algorithms. The commutation clock cycles for the RSPC and NSPC are set at 5 kHz. The values of the factors and constants of the command strategy and the adaptation algorithm are available in Table 2. The effectiveness of the designed NFPC_ABC-PE is gauged by subjecting them to a symmetrical 3-phase short-circuit fault on the cable used for transmission, followed by a comparison with the results obtained from a NFPC_SMC as outlined in [31]. The time taken for a symmetrical 3-phase short-circuit fault is set at 200 ms, i.e. between $t = 2$ s and $t = 2.2$ s, as pictured in Figure 7 below.

A. RESULTS AT THE NETWORK

During the occurrence of a fault with the NFPC_ABC-PE and NFPC_SMC strategies, the active power at the NIP registers a decrease below zero, as in Figure 8. This implies that the fault event leads to a reduction in the active power at the specified location in the electrical system. However, throughout the remaining fault duration, these two command strategies contribute to enhancing this power. In contrast to the NFPC_SMC strategy, the results shown in Figure 9 clearly demonstrate that NSPC, which incorporates the proposed strategy, is capable of providing a significant supply of reactive energy. This supply is crucial for maintaining operational stability, not

TABLE 1. DFIG parameter values.

Parameter	Value
P_n	2 MW
V_{sn}	690 V
f	50 Hz
p	2
R_s	0.023 pu
R_r	0.016 pu
L_s	0.18 pu
L_r	0.18 pu
L_m	2.9 pu
V_{dc}	1.2 kV

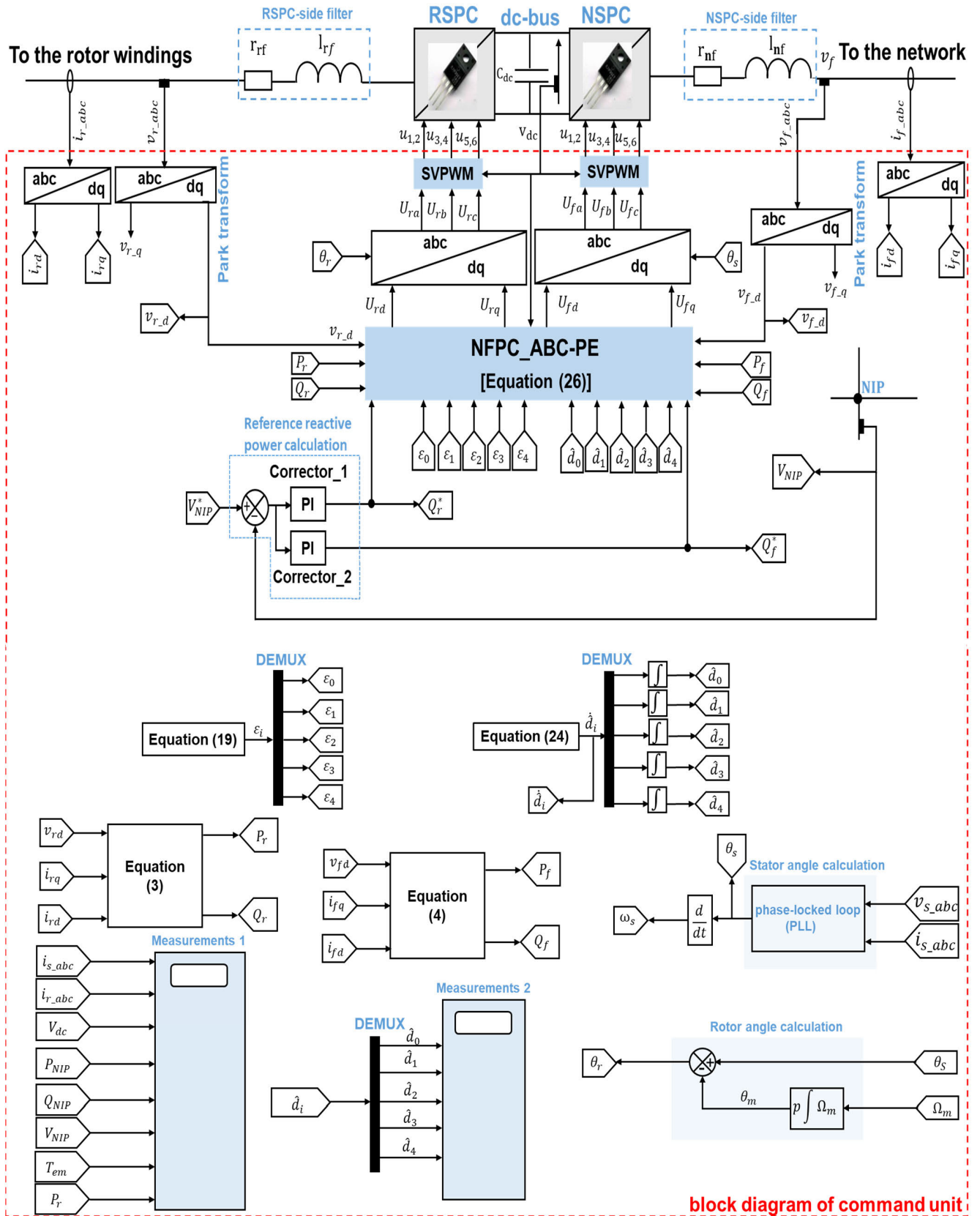
* pu: per unit

only during fault onset, but also in subsequent steady-state operations.

Figure 10 illustrates the NIP voltage responses when employing the proposed strategy during a fault period. The use of NFPC_ABC-PE results in a notably improved recovery of NIP voltage during faults, displaying an optimal short transient regime upon network voltage restoration. This improvement, unlike NFPC_SMC, contributes to an enhanced FRT capacity. In contrast, NFPC_SMC exhibits a more modest recovery during faults and has a slow response time upon network voltage recovery, which no longer aligns

$$\begin{aligned} \dot{V}_1(\varepsilon_i, \tilde{d}_i) = & -c_0\varepsilon_0^2 + \varepsilon_1 \left(-\hat{d}_1 P_r - \omega_s Q_r - \hat{d}_2 (v_{rd} V_{dc} U_{rd} - v_{rd}^2) - M_0 \hat{d}_0 + N_0 \right) + \varepsilon_2 \left(-\hat{d}_1 Q_r + \omega_s P_r - \hat{d}_2 v_{rd} V_{dc} U_{rq} - Q_r^* \right) \\ & + \varepsilon_3 \left(-\hat{d}_3 P_f - \omega_s Q_f - \hat{d}_4 (v_{fd} V_{dc} U_{fd} - v_{fd}^2) - M_1 \hat{d}_0 + N_1 \right) + \varepsilon_4 \left(-\hat{d}_3 Q_f + \omega_s P_f - \hat{d}_4 v_{fd} V_{dc} U_{fq} - Q_f^* \right) \\ & - \frac{\tilde{d}_0}{\beta_0} \left(\dot{\hat{d}}_0 - \mu + \beta_0 (M_0 \varepsilon_1 + M_1 \varepsilon_3) \right) - \frac{\tilde{d}_1}{\beta_1} \left(\dot{\hat{d}}_1 + \beta_1 (\varepsilon_1 P_r + \varepsilon_2 Q_r) \right) \\ & - \frac{\tilde{d}_2}{\beta_2} \left(\dot{\hat{d}}_2 + \beta_2 \varepsilon_1 (v_{rd} V_{dc} U_{rd} - v_{rd}^2) + \beta_2 \varepsilon_2 v_{rd} V_{dc} U_{rq} \right) - \frac{\tilde{d}_3}{\beta_3} \left(\dot{\hat{d}}_3 + \beta_3 (\varepsilon_3 P_f + \varepsilon_4 Q_f) \right) \\ & - \frac{\tilde{d}_4}{\beta_4} \left(\dot{\hat{d}}_4 + \beta_4 \varepsilon_3 (v_{fd} V_{dc} U_{fd} - v_{fd}^2) + \beta_4 \varepsilon_4 v_{fd} V_{dc} U_{fq} \right) \end{aligned} \quad (23)$$

$$\begin{aligned} \dot{V}_1(\varepsilon_i, \tilde{d}_i) = & -c_0\varepsilon_0^2 + \varepsilon_1 \left(-\hat{d}_1 P_r - \omega_s Q_r - \hat{d}_2 (v_{rd} V_{dc} U_{rd} - v_{rd}^2) - M_0 \hat{d}_0 + N_0 \right) + \varepsilon_2 \left(-\hat{d}_1 Q_r + \omega_s P_r - \hat{d}_2 v_{rd} V_{dc} U_{rq} - Q_r^* \right) \\ & + \varepsilon_3 \left(-\hat{d}_3 P_f - \omega_s Q_f - \hat{d}_4 (v_{fd} V_{dc} U_{fd} - v_{fd}^2) - M_1 \hat{d}_0 + N_1 \right) + \varepsilon_4 \left(-\hat{d}_3 Q_f + \omega_s P_f - \hat{d}_4 v_{fd} V_{dc} U_{fq} - Q_f^* \right) \end{aligned} \quad (25)$$



block diagram of command unit

FIGURE 6. The synoptic scheme of the command strategy of the RSPC and NSPC-side filters.

TABLE 2. Factors and constants in the NFPC_ABC-PE conceived.

c_0	c_1	c_2	c_3	c_4	β_0	β_1	β_2	β_3	β_4
11	6	8	14	13	7	9	11	4	10

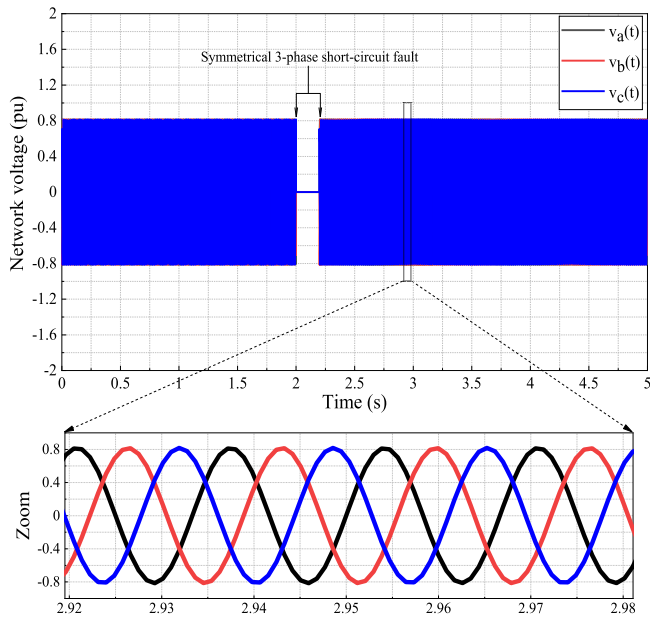


FIGURE 7. Network voltage affected by a fault.

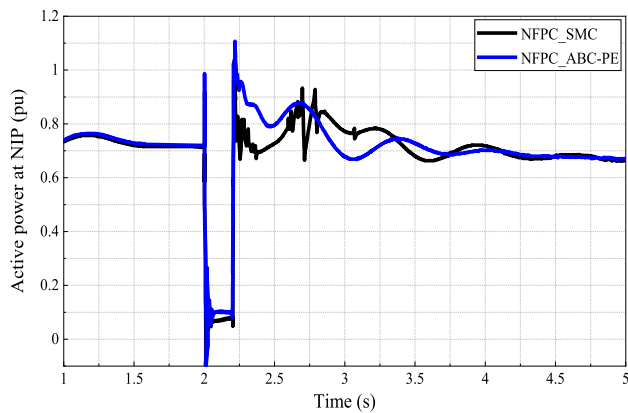


FIGURE 8. Active power at NIP.

with the WP voltage requirements (specified in the proprietary network code) necessary for sustained online operation following a network failure.

B. RESULTS AT THE WIND PARK

In Figures 11 and 12, the stator and rotor current responses are depicted under two distinct commands: (a) NFPC_SMC strategy and (b) NFPC_SMC strategy during a fault. The stator overcurrent that existed during the fault exceeded the accepted limit ($<2pu$) using the NFPC_SMC strategy when the fault was tripped (reached $3.5pu$) and cleared

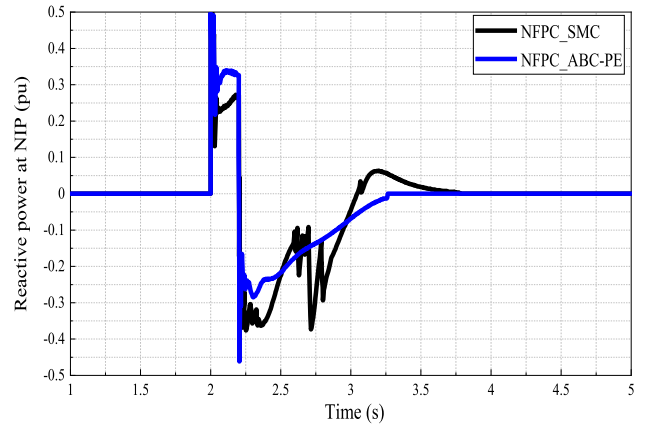


FIGURE 9. Reactive power at NIP.

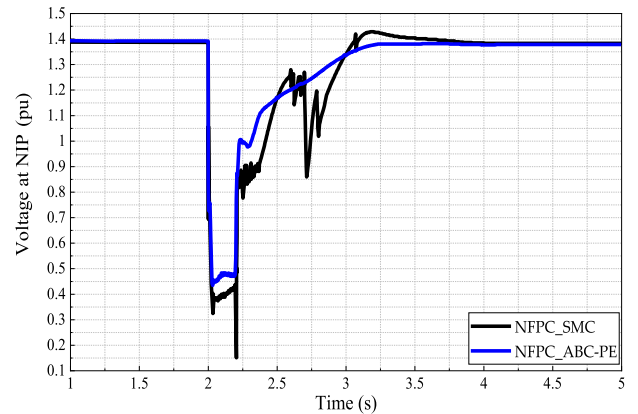


FIGURE 10. Voltage at NIP.

(reached $2pu$). Moreover, both deformation and current elimination can also be observed during the fault. Indeed, using the NFPC_ABC-PE strategy, the surge current is limited to less than $1.6pu$ at fault onset and $<2pu$ at fault clearing. Moreover, during the fault, the current is available and retains its sinusoidal form (see zoom in Figure 11b). Similarly, the effect of the stator current is transferred to the rotor through the electromagnetic coupling of their windings.

The utilization of the NFPC_SMC strategy results in the induction of an overcurrent during a fault scenario, surpassing the established safety threshold of the RSPC, which is specified to be less than 1.5 per unit (pu) based on the data sheet for power electronic components. Specifically, when the fault occurs and reaches a magnitude of 5 pu, and subsequently, when it is cleared and drops to 2.1 pu, the overcurrent condition arises, breaching the safety limit.

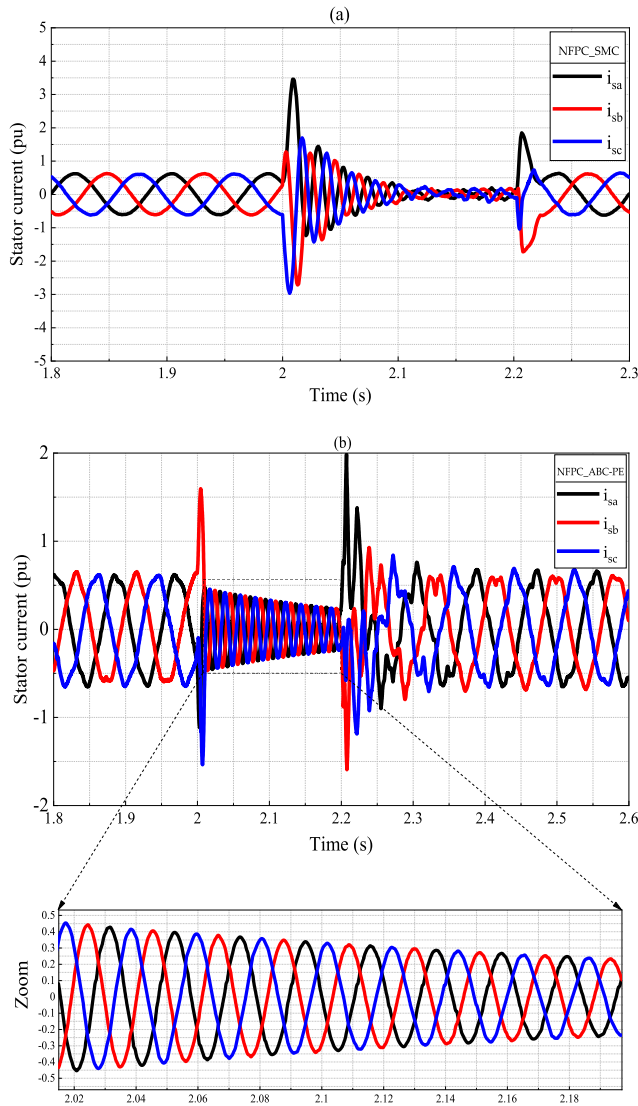


FIGURE 11. Stator current.

Moreover, aside from the overcurrent issue, additional phenomena are observed during the fault period. Deformation and current cancellation effects are discernible, indicating complex behaviors within the system beyond mere overcurrent concerns. These observations highlight the intricate nature of fault scenarios in power systems and underscore the necessity for robust control strategies to effectively manage such situations while maintaining system stability and safety.

Certainly, with the implementation of the NFPC_ABC-PE strategy, the overcurrent is restricted to less than 1.5pu at fault onset and at the fault clearance time. This demonstrates that the RSPC is operating within its established safety range.

In addition, the current is available during the fault and retains its original sinusoidal form (see zoom in Figure 12b). In Figure 13, the application of the NFPC-SMC strategy is revealed by the appearance of an overvoltage at the dc-bus terminals during the fault and a prolonged transient

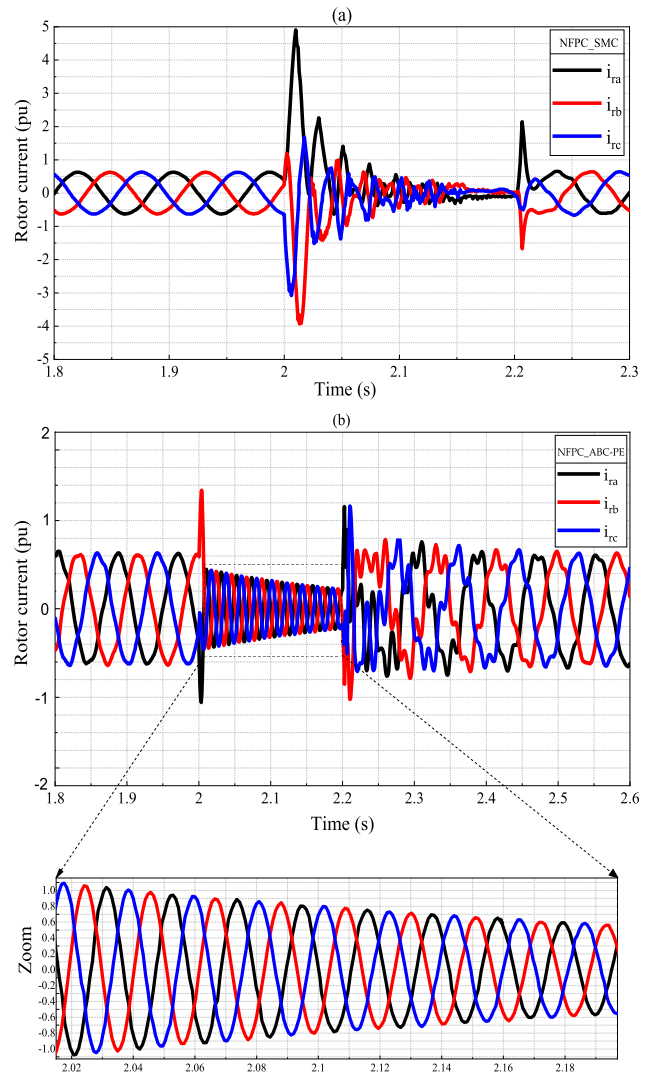


FIGURE 12. Rotor current.

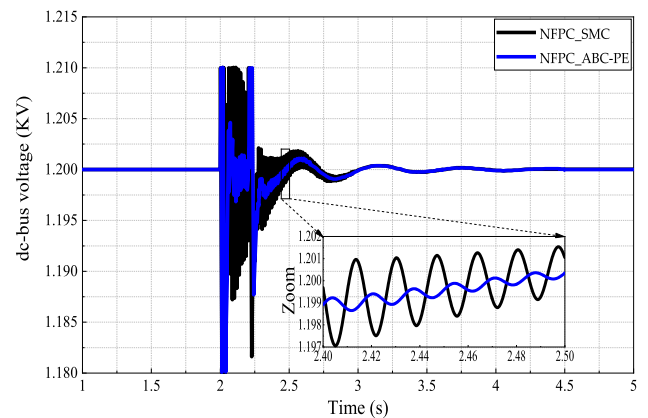


FIGURE 13. Voltage between dc-bus.

regime marked by significant oscillations after the fault has been recovered. The limitations of this strategy can be addressed through the proposed NFPC_ABC-PE strategy,

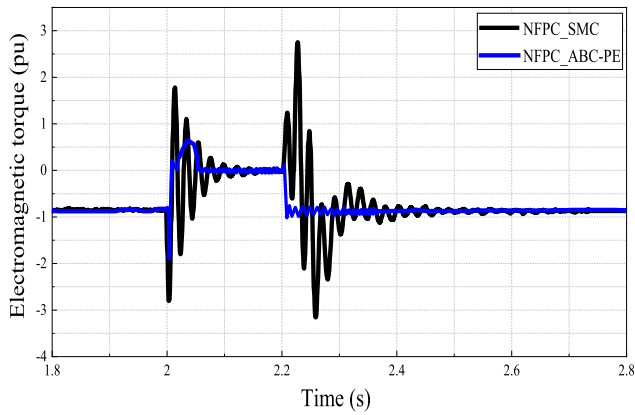


FIGURE 14. Electromagnetic torque.

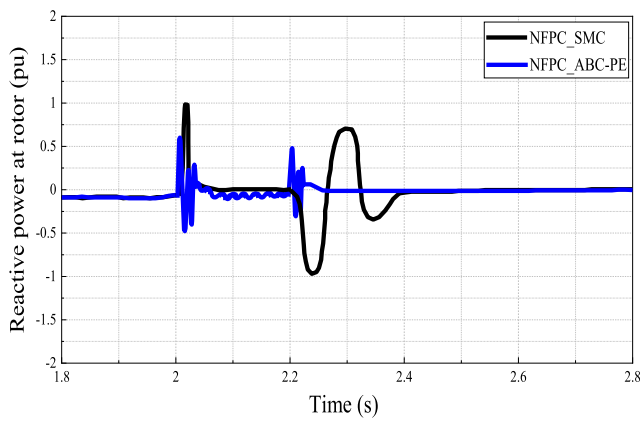


FIGURE 15. Reactive power at rotor.

which effectively controls overvoltage during faults, shortens the transient regime, and minimizes oscillations (zoom in Figure 13).

In Figure 14, with NFPC-SMC the transient electromagnetic torque in both the rotor and stator initially rises negatively until reaching 2.8pu, then swiftly transitions to a positive increase, reaching 1.8pu. It initiates oscillation at 2.1s, eventually dipping to 2.8pu in the negative direction, followed by a rapid rise and stabilization post-grid voltage recovery at 2.4s, marked by a reduced number of oscillations.

However, NFPC_ABC-PE demonstrates a more noticeable enhancement in minimizing peak oscillations both during and after mains voltage restoration. The rotor reactive power results are depicted in Figure 15. Under the NFPC-SMC, it reaches a value of 1pu initially, then swiftly returns to 0pu for the remainder of the fault. Upon voltage restoration in the network, a significant oscillation is observed in the transient regime, extending up to 1.4s. Nonetheless, NFPC_ABC-PE demonstrates a more substantial enhancement in reducing reactive power consumption at the onset of a fault and minimizing oscillations following mains voltage restoration.

Utilizing the estimated values presented in Figure 16, the designed NFPC_ABC-PE incorporates all parameters in the

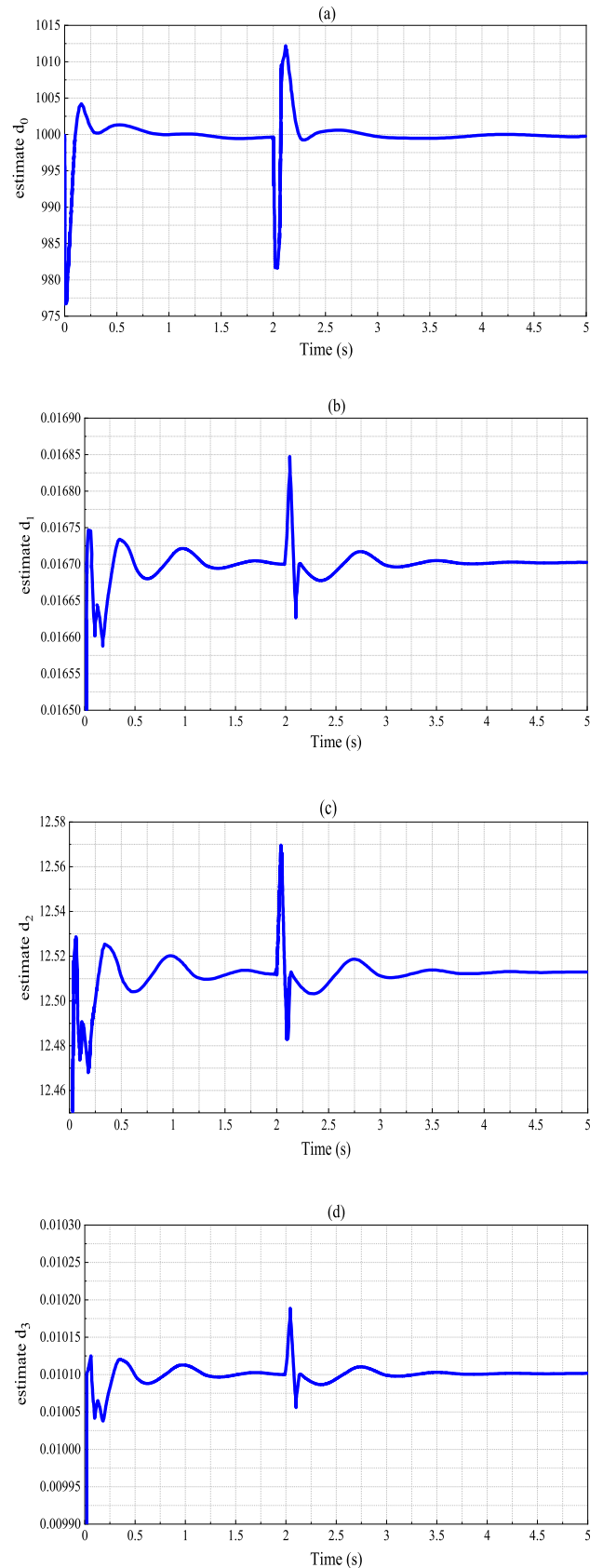


FIGURE 16. Parameters estimation.

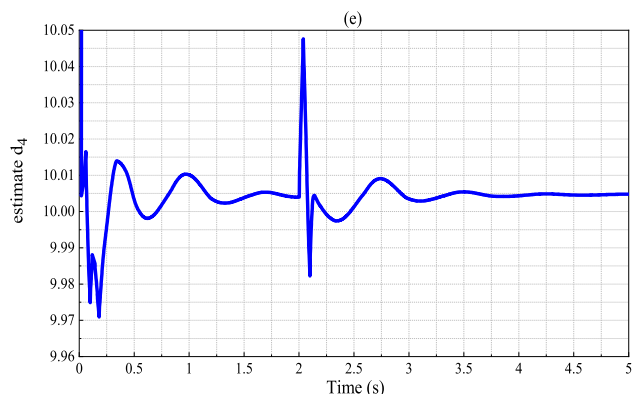


FIGURE 16. (Continued.) Parameters estimation.

model. This figure illustrates the disturbance in estimated values under fault conditions. However, once the fault has been eliminated, these estimated values stabilize back to them before fault levels. The effectiveness of the command system designed to estimate unknown parameters is evident in all these figures, highlighting the robustness of NFPC_ABC-PE to parametric variation during fault.

VI. ADDITIONAL DISCUSSION

In this research study, the NFPC_ABC-PE control strategy showcases commendable efficiency, effectiveness, and precision in the WP:

- **Efficiency:** The NFPC_ABC-PE demonstrates high efficiency by effectively managing and optimizing the operation of the WP. Its ability to enhance reactive power injection and facilitate voltage stabilization indicates efficient utilization of resources and improved system performance.
- **Effectiveness:** The NFPC_ABC-PE proves highly effective in comparison to the NFPC_SMC strategy. It successfully minimizes current fluctuations and ensures stable dc-bus voltage levels, indicating its capability to address key challenges faced by DFIG-based WPs. This effectiveness highlights its potential to mitigate system vulnerabilities and enhance overall operational reliability.
- **Precision:** The NFPC_ABC-PE precision in resolving system issues is noteworthy. Its ability to precisely control reactive power injection and voltage stabilization contributes to the system's stability and reliability. The comparison with NFPC_SMC underscores the precision of NFPC_ABC-PE in achieving desired control objectives with improved performance metrics.

Overall, the evaluation demonstrates that the NFPC_ABC-PE control strategy is not only efficient but also highly effective and precise in resolving critical issues within DFIG-based WPs. Its potential to enhance FRT capacity further solidifies its position as a promising control strategy for optimizing the performance and reliability of WP.

VII. CONCLUSION

A novel nonlinear scheme for forward power command is designed for DFIG-based WPs, allowing simultaneous control of both active and reactive output power at both the RSPC and NSPC-side filters. The approach is based on dynamic models of RSPC and NSPC-side filters, where all variables are expressed in terms of active and reactive power.

The applied NFPC_ABC-PE guarantees accurate monitoring of both active and reactive power for both RSPC and NSPC-side filters, including the dc-bus voltage represented by the active power equalization equation. The full parameters, including filter settings and dc-bus condensers, are assumed to be entirely unknown and are estimated through the application of parameter adaptation algorithms. The parameter adaptation algorithms are derived from the final LF result, which ensures that estimation errors are minimized to zero. The command signals are calculated in a way that ensures the stability of the overall system is maintained. In-depth theoretical analyses are presented, backed up by rigorous validation and simulation research. The results of the MATLAB/SIMULINK simulation undeniably confirm that the NFPC_ABC-PE strategy developed increases the voltage at the NIP by providing substantial reactive power compared to the NFPC_SMC strategy used in other publications in the presence of a fault on the network. This enhancement significantly boosts the FRT capacity of DFIG-based WPs.

In the forthcoming phase of work, we will analyze the performance of the developed NFPC_ABC-PE under various fault modes, loads, and climatic conditions. The validation process will rely on experimental results.

REFERENCES

- [1] W. Srirattanawichaikul, S. Premrudeepreechacharn, and Y. Kumsuwan, "A comparative study of vector control strategies for rotor-side converter of DFIG wind energy systems," in *Proc. 13th Int. Conf. Electr. Eng./Electron., Comput., Telecommun. Inf. Technol. (ECTI-CON)*, Jun. 2016, pp. 1–6, doi: [10.1109/ECTICon.2016.7561468](https://doi.org/10.1109/ECTICon.2016.7561468).
- [2] R. Yan, T. K. Saha, F. Bai, and H. Gu, "The anatomy of the 2016 south Australia blackout: A catastrophic event in a high renewable network," *IEEE Trans. Power Syst.*, vol. 33, no. 5, pp. 5374–5388, Sep. 2018, doi: [10.1109/TPWRS.2018.2820150](https://doi.org/10.1109/TPWRS.2018.2820150).
- [3] A. Jalilian, S. B. Naderi, M. Negnevitsky, M. Tarafdar Hagh, and K. M. Muttaqi, "Controllable DC-link fault current limiter augmentation with DC chopper to improve fault ride-through of DFIG," *IET Renew. Power Gener.*, vol. 11, no. 2, pp. 313–324, Feb. 2017, doi: [10.1049/iet-rpg.2016.0146](https://doi.org/10.1049/iet-rpg.2016.0146).
- [4] J. J. Justo, F. Mwasilu, and J.-W. Jung, "Doubly-fed induction generator based wind turbines: A comprehensive review of fault ride-through strategies," *Renew. Sustain. Energy Rev.*, vol. 45, pp. 447–467, May 2015, doi: [10.1016/j.rser.2015.01.064](https://doi.org/10.1016/j.rser.2015.01.064).
- [5] J. Vidal, G. Abad, J. Arza, and S. Aurtenechea, "Single-phase DC crowbar topologies for low voltage ride through fulfillment of high-power doubly fed induction generator-based wind turbines," *IEEE Trans. Energy Convers.*, vol. 28, no. 3, pp. 768–781, Sep. 2013, doi: [10.1109/TEC.2013.2273227](https://doi.org/10.1109/TEC.2013.2273227).
- [6] A. Loulijat, H. Chojaa, M. El Marghichi, N. Ettalabi, A. Hilali, A. Mouradi, A. Y. Abdelaziz, Z. M. S. Elbarbary, and M. A. Mossa, "Enhancement of LVRT ability of DFIG wind turbine by an improved protection scheme with a modified advanced nonlinear control loop," *Processes*, vol. 11, no. 5, p. 1417, 2023.

- [7] A. Loulijat, "Crowbar with a parallel RpLp configuration using PI controller to solve the problem of DFIG-wind farm stability during a symmetrical fault," *Int. J. Intell. Eng. Syst.*, vol. 16, no. 6, pp. 799–812, 2023, doi: [10.22266/ijies2023.1231.66](https://doi.org/10.22266/ijies2023.1231.66).
- [8] G. Pannell, B. Zahawi, D. J. Atkinson, and P. Missailidis, "Evaluation of the performance of a DC-link brake chopper as a DFIG low-voltage fault-ride-through device," *IEEE Trans. Energy Convers.*, vol. 28, no. 3, pp. 535–542, Sep. 2013, doi: [10.1109/TEC.2013.2261301](https://doi.org/10.1109/TEC.2013.2261301).
- [9] O. S. Adekanle, M. Guisser, E. Abdelmounim, and M. Aboufatah, "Non-linear controller with rotor crowbar and DC-chopper fault ride through technique for grid-connected doubly fed induction generator," *Int. Rev. Autom. Control*, vol. 11, pp. 281–292, Nov. 2018.
- [10] A. Loulijat, O. S. Adekanle, H. F. Fassi, and N. Ababssi, "Wind farms use DFIG with a passive method of protection against grid faults," in *Proc. Int. Conf. Wireless Technol., Embedded Intell. Syst. (WITS)*, Apr. 2019, pp. 1–7, doi: [10.1109/WITS.2019.8723844](https://doi.org/10.1109/WITS.2019.8723844).
- [11] M. E. Hossain, "Low voltage ride-through capability improvement methods for DFIG based wind farm," *J. Electr. Syst. Inf. Technol.*, vol. 5, no. 3, pp. 550–561, Dec. 2018, doi: [10.1016/j.jesit.2017.12.002](https://doi.org/10.1016/j.jesit.2017.12.002).
- [12] A. Causebrook, D. J. Atkinson, and A. G. Jack, "Fault ride-through of large wind farms using series dynamic braking resistors (March 2007)," *IEEE Trans. Power Syst.*, vol. 22, no. 3, pp. 966–975, Aug. 2007, doi: [10.1109/TPWRS.2007.901658](https://doi.org/10.1109/TPWRS.2007.901658).
- [13] J. Shi, Y. Tang, Y. Xia, L. Ren, and J. Li, "SMES based excitation system for doubly-fed induction generator in wind power application," *IEEE Trans. Appl. Supercond.*, vol. 21, no. 3, pp. 1105–1108, Jun. 2011, doi: [10.1109/TASC.2011.2105450](https://doi.org/10.1109/TASC.2011.2105450).
- [14] T. K. Roy, M. A. Mahmud, S. N. Islam, K. M. Muttaqi, and A. M. T. Oo, "Nonlinear adaptive direct power controllers of DFIG-based wind farms for enhancing FRT capabilities," in *Proc. IEEE Ind. Appl. Soc. Annu. Meeting*, Sep. 2019, pp. 1–6, doi: [10.1109/IAS.2019.8912407](https://doi.org/10.1109/IAS.2019.8912407).
- [15] Z.-C. Zou, X.-Y. Xiao, Y.-F. Liu, Y. Zhang, and Y.-H. Wang, "Integrated protection of DFIG-based wind turbine with a resistive-type SFCL under symmetrical and asymmetrical faults," *IEEE Trans. Appl. Supercond.*, vol. 26, no. 7, pp. 1–5, Oct. 2016, doi: [10.1109/TASC.2016.2574352](https://doi.org/10.1109/TASC.2016.2574352).
- [16] K. E. Okedu, S. M. Muyeen, R. Takahashi, and J. Tamura, "Wind farms fault ride through using DFIG with new protection scheme," *IEEE Trans. Sustain. Energy*, vol. 3, no. 2, pp. 242–254, Apr. 2012, doi: [10.1109/TSST.2011.2175756](https://doi.org/10.1109/TSST.2011.2175756).
- [17] A. Rini Ann Jerin, P. Kaliannan, and U. Subramaniam, "Improved fault ride through capability of DFIG based wind turbines using synchronous reference frame control based dynamic voltage restorer," *ISA Trans.*, vol. 70, pp. 465–474, Sep. 2017, doi: [10.1016/j.isatra.2017.06.029](https://doi.org/10.1016/j.isatra.2017.06.029).
- [18] A. Touati, E. Abdelmounim, M. Aboufatah, A. Moutabir, and R. Majdoul, "Improved strategy of an MPPT based on the torque estimator for variable speed turbines," *Int. Rev. Model. Simul.*, vol. 8, no. 6, pp. 620–631, 2015, doi: [10.15866/iremos.v8i6.7122](https://doi.org/10.15866/iremos.v8i6.7122).
- [19] D. Zhang, H. Xu, L. Qiao, and L. Chen, "LVRT capability enhancement of DFIG based wind turbine with coordination control of dynamic voltage restorer and inductive fault current limiter," *PLoS ONE*, vol. 14, no. 8, Aug. 2019, Art. no. e0221410, doi: [10.1371/journal.pone.0221410](https://doi.org/10.1371/journal.pone.0221410).
- [20] Md. A. Chowdhury, Md. A. Mahmud, W. Shen, and H. R. Pota, "Nonlinear controller design for series-compensated DFIG-based wind farms to mitigate subsynchronous control interaction," *IEEE Trans. Energy Convers.*, vol. 32, no. 2, pp. 707–719, Jun. 2017, doi: [10.1109/TEC.2017.2660539](https://doi.org/10.1109/TEC.2017.2660539).
- [21] S. S. A. Alhalim and L. A. Alnabi, "Enhancement transient stability of wind power system of doubly-fed induction generator using STATCOM and PI controller," *Int. J. Power Electron. Drive Syst.*, vol. 10, no. 4, pp. 1977–1985, 2019, doi: [10.11591/ijpeds.v10.i4.pp1977-1985](https://doi.org/10.11591/ijpeds.v10.i4.pp1977-1985).
- [22] N. Ababssi, E. A. Semma, and A. Loulijat, "Implementation optimal location of STATCOM on the IEEE New England power system grid (100 kV)," *Int. J. Intell. Eng. Syst.*, vol. 15, no. 3, pp. 441–454, 2022, doi: [10.22266/ijies2022.0630.37](https://doi.org/10.22266/ijies2022.0630.37).
- [23] H. Abu-Rub, M. Malinowski, and K. Al-Haddad, "Power electronics for renewable energy systems," in *Transportation and Industrial Applications*. Hoboken, NJ, USA: Wiley, 2014, doi: [10.1002/9781118755525](https://doi.org/10.1002/9781118755525).
- [24] R. Pena, J. C. Clare, and G. M. Asher, "Doubly fed induction generator using back-to-back PWM converters and its application to variable-speed wind-energy generation," *IEE Proc.-Electr. Power Appl.*, vol. 143, no. 3, pp. 231–241, 1996, doi: [10.1049/ip-epa:19960288](https://doi.org/10.1049/ip-epa:19960288).
- [25] G. Li and L. Hang, "Control of doubly-fed induction generators for wind turbines," in *Modeling and Modern Control of Wind Power*. Hoboken, NJ, USA: Wiley, 2018, pp. 37–62, doi: [10.1002/9781119236382.ch3](https://doi.org/10.1002/9781119236382.ch3).
- [26] H. Benbouhenni, E. Bounadja, H. Gasmı, N. Bizon, and I. Colak, "A new PD(1+PI) direct power controller for the variable-speed multi-rotor wind power system driven doubly-fed asynchronous generator," *Energy Rep.*, vol. 8, pp. 15584–15594, Nov. 2022, doi: [10.1016/j.egy.2022.11.136](https://doi.org/10.1016/j.egy.2022.11.136).
- [27] H. Farhangi, "Smart grid system integration," *Smart Microgrids*, vol. 7, no. 1, pp. 31–63, 2016, doi: [10.1201/9781315372679-3](https://doi.org/10.1201/9781315372679-3).
- [28] K. Reddy and A. K. Saha, "A heuristic approach to optimal crowbar setting and low voltage ride through of a doubly fed induction generator," *Energies*, vol. 15, no. 24, p. 9307, Dec. 2022, doi: [10.3390/en15249307](https://doi.org/10.3390/en15249307).
- [29] S. Kammoun, S. Sallem, and M. B. A. Kammoun, "Backstepping control for low-voltage ride through enhancement of DFIG-based wind turbines," *Arabian J. Sci. Eng.*, vol. 42, no. 12, pp. 5083–5099, Dec. 2017, doi: [10.1007/s13369-017-2606-z](https://doi.org/10.1007/s13369-017-2606-z).
- [30] O. Adekanle, M. Guisser, E. Abdelmounim, and M. Aboufatah, "Adaptive backstepping control of grid-connected doubly-fed induction generator during grid voltage dip," in *Proc. Int. Conf. Electr. Inf. Technol. (ICEIT)*, Nov. 2017, pp. 1–6, doi: [10.1109/EITech.2017.8255267](https://doi.org/10.1109/EITech.2017.8255267).
- [31] A. Loulijat, M. El marghichi, and S. Abbou, "Secures and maintains non-linear control of DFIG-wind turbine by implementing the appropriate protection configuration against overcurrent in the rotor circuit under grid fault," in *Proc. E3S Web Conf.*, 2023, pp. 1–14.
- [32] T. K. Roy, M. A. Mahmud, S. N. Islam, and A. M. T. Oo, "Direct power controller design for improving FRT capabilities of DFIG-based wind farms using a nonlinear backstepping approach," in *Proc. 8th Int. Conf. Power Energy Syst. (ICPES)*, Dec. 2018, pp. 240–245, doi: [10.1109/ICPESYS.2018.8626979](https://doi.org/10.1109/ICPESYS.2018.8626979).
- [33] Md. R. Islam, J. Hasan, Md. R. R. Shipon, M. A. H. Sadi, A. Abuhusseini, and T. K. Roy, "Neuro fuzzy logic controlled parallel resonance type fault current limiter to improve the fault ride through capability of DFIG based wind farm," *IEEE Access*, vol. 8, pp. 115314–115334, 2020, doi: [10.1109/ACCESS.2020.3000462](https://doi.org/10.1109/ACCESS.2020.3000462).
- [34] G. S. Kaloi, J. Wang, and M. H. Baloch, "Active and reactive power control of the doubly fed induction generator based on wind energy conversion system," *Energy Rep.*, vol. 2, pp. 194–200, Nov. 2016, doi: [10.1016/j.egy.2016.08.001](https://doi.org/10.1016/j.egy.2016.08.001).
- [35] A. Loulijat, N. Ababssi, and M. Mohamed, "Kalman observer contribution to a second order sliding mode control for wind turbine based on DFIG during the network voltage dip," *Int. J. Intell. Eng. Syst.*, vol. 14, no. 5, pp. 88–101, Oct. 2021, doi: [10.22266/ijies2021.1031.09](https://doi.org/10.22266/ijies2021.1031.09).



AZEDDINE LOULIJAT was born in Settat, Morocco. He received the master's degree in automatic, signal processing and industrial computing from the Science and Technical Faculty, Hassan 1st University, Settat, in 2014, where he is currently pursuing the Ph.D. degree with the Laboratory of Engineering, Industrial Management and Innovation. His Ph.D. thesis titled "Impact of Perturbations of High Voltage Grids on Wind System Performance: Control and Observation." His research focuses on linear and nonlinear control using advanced controllers with observers in the energy domain, notably wind power linked electric grid.

MOHAMED MAKHAD was born in Agadir, Morocco. He received the master's degree in electrical engineering from the Higher Normal School of Technical Education, Rabat. He is currently pursuing the Ph.D. degree in electrical engineering with Mohammed V University. His current research interests include solar energy systems, wind energy conversion systems, microgrids, optimization algorithm for energy management systems, sliding mode control, and robust control of dynamical systems.

ABDELILAH HILALI is a Doctor in the Faculty of Sciences at the Moulay Ismail University in Meknes, Morocco, and an Associate Teacher of Electrical Engineering at CPGE-Settat, Morocco. His research focuses on the sizing of electrical installations, the optimization of their operation and the search for solutions to improve the performance or increase the efficiency of an electrical system, such as maximum power point trackers (MPPT) or optimization through the insertion of storage devices such as batteries or flywheels. His research interests also include the development of advanced control strategies (control of maximum power point trackers by metaheuristic methods or using artificial intelligence; control of electrical machines such as DTC, MRAS, depending on the type of application such as solar pumping, hybrid vehicles or power grids).

HAMID CHOJAA was born in Settat, Morocco, in 1990. He received the master's degree in science and technology from Hassan 1st University, in 2014. His master's thesis titled on "Automatic Control, Signal Processing and Industrial Computing." He is currently working on a doctoral thesis with the Electrical Engineering Department, Higher School of Technology, USMBA University, Fes. His main research interests include renewable energy, machine control, and electrical systems.

MOUNCEF EL MARGHICHI received the degree from ENSA Marrakech and the Ph.D. degree from the Faculty of Science and Technology, Settat. He is a dedicated electrical engineer. Currently, he is an Assistant Professor with the Faculty of Sciences, Tetouan. His research focuses on developing algorithms for state of charge, health estimation of lithium batteries, and battery management systems. Additionally, he has made significant contributions to the field of photovoltaic modeling through the creation of advanced algorithms. With a robust background in electrical engineering and expertise in algorithm development, he is committed to advancing the fields of energy storage and renewable energy systems.

MOHAMMED HATATAH received the B.Sc. degree in electrical engineering and the M.B.A. degree from King Abdulaziz University, Saudi Arabia, in 2007 and 2010, respectively, the M.Sc. degree in power system from The Pennsylvania State University, USA, in 2015, and the Ph.D. degree in power electronics from the University of Pittsburgh, USA, in 2021. In 2005, he did a six months internship with Saudi Aramco, Saudi Arabia, where he worked on distribution equipment design. From 2006 to 2011, he was an Electrical Planning Engineer with Saudi Electricity Company, Saudi Arabia, where he worked on the regional planning (110kV). His research interests include power systems, renewable energy, and control and optimization of power converter. He is a member of IEEE PELS and PES.

THAMER A. H. ALGHAMDI received the B.Sc. degree from Al-Baha University, Al-Baha, Saudi Arabia, in 2012, the M.Sc. degree from Northumbria Newcastle University, Newcastle upon Tyne, U.K., in 2016, and the Ph.D. degree from Cardiff University, Cardiff, U.K., in 2023. He is an Assistant Professor of electrical power engineering with the Electrical Engineering Department, Al-Baha University. He was a Power Distribution Engineer with Saudi Electricity Company (SEC), until 2013. He was a Lecturer Assistant with Al-Baha University, from 2016 to 2018. His main research interests include power systems, power quality, the integration of renewables, and AI applications in electrical power engineering.

• • •